Entropy-Based Cavitation and Primary Atomization Analysis with a 2D Transparent Injector

Jean-Bernard Blaisot, Fakhry Abuzahra, Akira Sou, Christophe Dumouchel

HAL Id: hal-02271672

https://normandie-univ.hal.science/hal-02271672

Submitted on 16 Oct 2019

Entropy-based cavitation and primary atomization analysis with a 2D transparent injector

Jean-Bernard Blaisot*[1], Fakhry Abuzahra[1], Akira Sou[2], Christophe Dumouchel[1]

[1]CORIA – UMR 6614, Normandie Université, Université et INSA de Rouen, Saint-Etienne du Rouvray, France

[2]Kobe University, Japan

*Corresponding author: blaisot@coria.fr

Abstract

A transparent scale-up injector with asymmetric incoming flow direction was designed to promote cavitation on mainly one-side of the orifice. This orifice has a rectangular cross-section that provides straightforward optical access to the internal flow. This geometry was designed to study the role of the internal flow, and particularly of the development of cavitation, on the modification of the primary atomization process occurring as soon as the liquid emanates from the injector.

The internal flow is classified into four regimes based on the extent of the cavitation zone; 1- no-cavitation, 2- developing cavitation, 3- super cavitation and 4- semi-hydraulic flip cavitation. Image series of 500 images was recorded for different flow rates belonging to regimes 2-4. Image segmentation is applied to each individual image to identify liquid and vapour phase regions. Based on these segmented images, the mean and rms values of the cavitation extent are determined for each cavitating regime. Furthermore, a more detailed statistical analysis of the cavitation is obtained with the computation of an entropy image, bringing indication on interface between vapour and liquid and on the shed cavitation bubbles.

The liquid jet fragmentation is qualified from the entropy analysis also. The primary atomization is associated with the region in the image where the liquid core is fragmented in detached ligaments and drops. This region is easily identified from the entropy analysis and the primary atomization is quantified through the computation of the area of this region.

In the presence of cavitation, the primary atomization process is altered. The way liquid fragmentation is modified by cavitation is shown to be correlated to the extent of the cavitation zone in the orifice. In this paper we give a quantification of these modifications, clearly visible to the naked eye on the images.

Keywords

Experiment; Image Analysis; Cavitation; Primary Atomization; Entropy

Introduction

Atomization processes and particularly primary atomization in the near field of the nozzle orifice of an injector are strongly linked to the properties of the flow inside the nozzle. The large velocity and pressure changes occurring in fuel injector nozzles trigger cavitation inception in region where the fluid undergoes low pressure or high viscous stresses [1]. It is well known that the cavitation influences the flow downstream the nozzle. It can lead to a change in spray cone angle [2] and spray contour shapes [3] and the way cavitation is developing in the nozzle closely affects the characteristics of the spray in the near field [4].

Characterizing the internal flow is of great importance when cavitation investigation is concerned. The very small injector geometry accompanied with high pressure and correspondingly high flow velocity in commercial injectors make flow visualization an arduous task. Transparent nozzles of real size [4][5] introduce limitations in terms of injection pressure and require using refractive index-matching techniques to visualize internal flows. In such conditions, quantitative evaluation of cavitation properties is often limited. Scaled-up nozzles [6][7] are useful tools to figure out how cavitation develops in the nozzle and eventually affect atomization. 2D scaled-up nozzles are particularly well suited for complete and detailed visualization of cavitating flows.

Sou et al. [7] investigated a simplified up-scaled version of a VCO injector where an asymmetry transparent nozzle is employed. The flow entering the nozzle changes its direction suddenly at the orifice inlet. A recirculation zone appears, mainly, near the up-stream orifice wall [8]. As the velocity increases, the local pressure decreases and the local viscous shear increases that promotes cavitation inception and, thus, bubbles start to appear [9]. The cavitation cloud extends as the velocity increases. Ligament structures was also observed by Sou et al. [10] mainly on the upstream side of the jet (the same side where the cavitation develops).

In this work, a scaled-up 2D transparent injector of identical geometry to the one of Sou et al. [10] is used to visualize internal and external flow utilizing high resolution images. These images are segmented to identify the liquid and

the gas or vapour phases and series of 500 images are analysed. For such large image series, statistical tools are needed to derive relevant quantitative quantities. This task is achieved here through the entropy approach. Quantitative parameters are determined from the entropy maps and their variations versus the injection flow rates are interpreted.

In the first part of the paper the experimental test bench, the nozzle geometry and the different flow regimes are presented. Then the entropy method is introduced. The internal flow and external flow analyses constitute the results and discussion part. The last section is dedicated to the central conclusion emerging out of the present study.

Experimental test bench

The scheme of the experimental rig is shown in Figure 1. The flow is driven by a centrifugal pump with a fixed flow rate $Q_{Tot} = 0.5$ m³/hr and a maximum injection pressure of 10 bar. The flowrate Q_m is controlled by a regulating valve and measured by a Coriolis-type flow meter. The working fluid, water at ambient temperature, is softened to eliminate the limestone. The operating conditions are given in Table 1, the varying parameter of the study being the flow rate $Q_m = Q_{Tot} - Q_{Reg}$ (see figure 1) where Q_{Reg} is the return flow controlled by the regulating valve. The mean flow velocity ($V_q = Q_m/(\rho_l A_N)$ where A_N is the orifice sectional area and ρ_l is the water density) is used to calculate gaseous Weber number We_g and Reynolds number Re, where the last is defined for the orifice thickness T_N=1 mm. The cavitation number CN is defined by $(P_{amb} - P_v)/(0.5\rho_l V_q^2)$ where P_{amb} is the ambient pressure and P_v is the saturation vapor pressure.
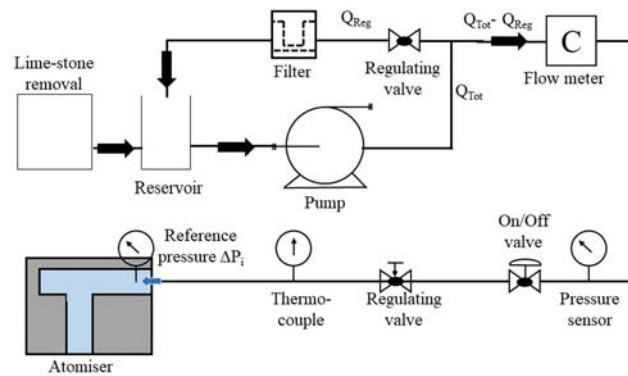

Figure 1. Experimental test rig

Table 1. Operating conditions: V_q is the mean flow velocity, ΔP_i is the differential (reference) injection pressure, Re is the Reynolds number, CN is the cavitation number and We_g is the gaseous Weber number.

Cond. N°	Q_m (10⁻³ kg/s)	V_q (m/s)	ΔP_i (bar)	Regime	Re	CN	We_g
1	40.0	10.0	1.35	I	10000	1.98	1.72
2	43.3	10.8	1.58	I	10850	1.69	2.02
3	47.5	11.9	1.86	II	11900	1.40	2.43
4	55.0	13.7	2.55	III	13750	1.05	3.25
5	57.5	14.4	2.83	III	14400	0.96	3.55
6	62.5	15.6	3.36	IV	15650	0.81	4.20
7	66.7	16.6	3.91	IV	16700	0.71	4.78
8	76.7	18.3	5.45	IV	19200	0.54	6.32

The injector was designed by Akira Sou [10]. Figure 2 shows a sketch of the 2D injector. The geometry is inspired from the internal path that the fuel follows in Valve Covered Orifice nozzles. Here the two main pipes are of rectangular cross-section of thickness T_N=1 mm. The supply pipe is horizontal and connected to the vertical discharging pipe (nozzle) of length L_N =16 mm and of width W_N=4 mm. The asymmetric in-flow with the angle of 90° between the supply pipe and the orifice, along with the sharp inlet, promote cavitation mainly on the upstream side of the nozzle. In the remainder, upstream and downstream terms will be relative to the supply pipe flow (see figure 2). The scaled-up injector favours cavitation at relative low injection pressure (7 bar) and low flow velocity (20 m/s).

A Diffuse Back Light (DBI) technique is employed to visualize internal and external flows (see figure 3). The optical setup consists of a short-pulsed illumination laser source (Quantel Ultra frequency doubled Q-Switched Nd:YAG, 532 nm), a high magnification objective (Nikkon 300 mm f/4D) coupled with an extension tube and high-resolution CCD camera (Dalsa Pantera 11M4). The image definition is 4016 x 2672 pixels. The magnification leads to a

corresponding physical field of 19.7 x 13.1 mm^2 with a spatial resolution of 4.9 μm/pixel. For each injection condition, a series of 500 images is recorded.

Four flow regimes have been observed: Regime I: no cavitation; Regime II: cavitation inception; Regime III: super cavitation; Regime IV: semi-hydraulic flip. The regimes are mainly differentiated by the extent length of the cavitation plume. Regime II corresponds to the appearance of cavitation bubbles at the entrance of the orifice. In the super cavitation regime (Regime III) the cavitation structures increases in length and may extend up to the nozzle exit. The semi-hydraulic flip regime (Regime IV) occurs when external air moves upstream in the orifice. This is induced by a cavitation plume that extends to the nozzle exit section and results in smoothed liquid jet interface. The regime is called "semi"-hydraulic flip here due to the nozzle asymmetry. These regimes are illustrated in figure 3. This figure shows that the atomization process is strongly modified with the flow rate and greatly relates with the development of the cavitation in the orifice.
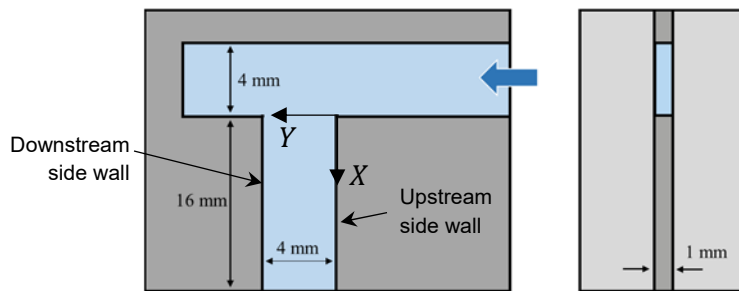
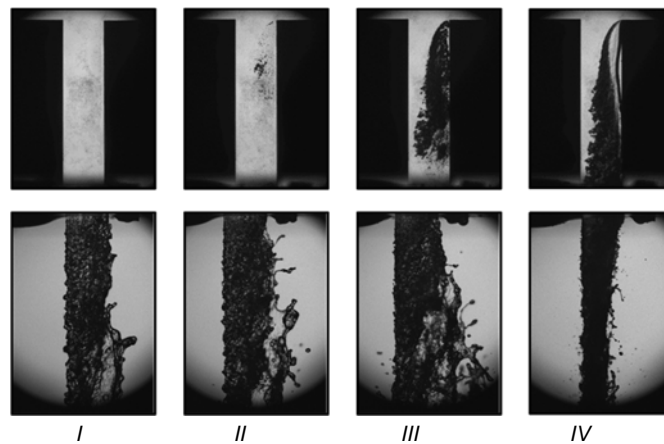

Figure 2. 2D transparent nozzle

Figure 3. Internal flow (upper row) and external flow (lower row) for the regime I to IV (from left to right)

Entropy method

The internal flow is characterized by a vapour phase dispersed in the surrounding liquid media and the external flow by a liquid phase fragmented in the surrounding air media. In this two-phase flow problem, the relevant phases are thus the liquid and the vapour or gas (air) phases. We will use the term liquid and gas phases in the remainder. In BDI images of the internal flow the light grey level represents the liquid phase and the dark grey level the gas phase whereas it is the opposite for the external flow (see figure 3). BDI images are segmented in two-level images on the basis of the grey level histogram corresponding to each phase, white pixels corresponding to the liquid and black pixels to the gas for the internal flow and inversely for the external flow.

To quantitatively characterize the cavitation in the nozzle and the atomization of the jet, and to analyse their statistical properties, an entropy-based approach using an home-made program is utilized [11]. The classical entropy definition derived from information theory is used here (see Eq. 1). It is based on the definition of 'states' to which the pixel belongs and specifically to the probability of occurrence of these states. The states are classically associated to the phases introduced before but an additional third state is also considered. For the internal flow the gas phase (black pixels) is actually divided in two states, i.e. cavitation plume (biggest vapour cavity) and the detached bubbles. For the external flow the liquid phase (black pixels) is divided in two states also, i.e. the jet (biggest liquid element) and the detached droplets. The probability p_s of occurrence of each state s ($s = L$ for liquid, $s = G$ for gas and $s = B$ for the biggest element) is computed over the image series for each pixel location. For this three-state condition, the entropy indicates how many states were seen by the pixels and what were their relative probability. The entropy is null as soon as only one state is seen by a pixel, whatever the state, and the maximum

entropy is reached when an equivalent probability is associated to each of the three states. This maximum serves to normalize entropy E values, i.e. maximum normalized entropy is 1:

$$E = \frac{-\sum_s p_s \, ln(p_s)}{ln(3)} \qquad (1)$$

Regions always covered by the liquid for the internal flow or by the gas for the external flow are thus assigned a null entropy value. Moreover, if there exist regions always occupied by the largest element, they will also be assigned a null value. Non-null entropy values correspond to region where at least two states occurred. This information could also be obtained by the fluctuation of presence of the liquid and gas phases. However, the advantage of the entropy quantity is that it does not depend on grey level values (due to the computation of probabilities) and it allows discriminating more than two states. Therefore, a criterion of interest concerning the occurrence of the three states at a given location is introduced. It is given by the 3-state entropy threshold E_3 below which only two states a and b occur, i.e. $p_a = p_b = 0.5$ and $p_c = 0$, leading to $E_3 = \frac{ln(2)}{ln(3)} \approx 0.631$. Pixels for which $E > E_3$ are concerned with the three states, i.e. the liquid, the gas and the biggest element are encountered at this location. For the internal flow, the corresponding region is located at the outline of the cavitation plume and is called the bubble detachment region. For the external flow these pixels are located at the outline of the jet, in a region of transition between continuous and fragmented liquid phases, referred to as the primary atomisation zone [11]. The quantitative analysis of the occurrence of the three states for the determination of the bubble detachment region or of the primary atomization zone can only be reached through the entropy quantity.

Internal flow analysis
As indicated in Table 1, conditions 1 and 2 lie in the 'no cavitation' regime I and are thus not selected for the analysis of the internal flow. Examples of segmented images are given in figure 4 where detached bubbles are represented in black and cavitation plume (biggest structure) is shown in blue. The statistics of the cavitation plume area A_B and of its centroid coordinates (X_B, Y_B) have been determined for condition 3-8. The results are presented in figure 5 as a function of the flow rate Q_m where dimensionless quantities are used, i.e. X_B is normalized by L_N, Y_B by W_N and A_B by the nozzle area $A_N = L_N \times W_N$. The results show that the mean value for A_B (figure 5-a) increases rapidly in the transition from regime II to regime IV. In regime II, the rms and mean value for A_B are almost the same, indicating that the vapour cavities are largely fluctuating in size for this condition corresponding to cavitation inception. In regime IV a plateau is reached for A_B that represents almost 70% of the nozzle orifice area. The gas phase is mainly constituted of one big bubble in this regime and the liquid represents only 30% of the nozzle area.


Cond. 3   *Cond. 4*   *Cond. 5*   *Cond. 6*   *Cond. 7*   *Cond. 8*
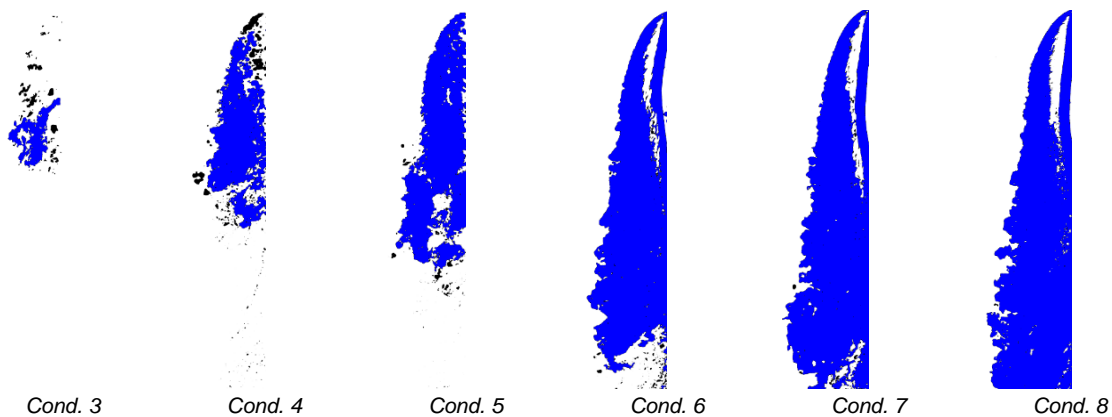
**Figure 4**. Internal flow: segmented image example for conditions 3 to 8. The cavitation plume is shown in blue.

The centroid location (figure 5-b) shows that the longitudinal location of the cavitation plume X_B depends on the regime whereas the transverse location Y_B does not and remains around one third of the nozzle width. The cavitation plume starts appearing at nozzle orifice entrance with a mean longitudinal location around 20% of the nozzle length characterized with very large fluctuation. As soon as regime IV is reached, the fluctuations of X_B are greatly reduced owing to the fact the cavitation plume totally covers the orifice length. X_B reaches the limit value of 0.55 as the plume is larger near the nozzle exit.
The entropy is evaluated from the segmented image series (see figure 4). The resulting entropy maps are presented in figure 6. As expected, the flow regions always occupied by the liquid have a null entropy. This corresponds to the black colour zone for condition 3. The coloured regions in entropy maps (i.e. non-null entropy values) correspond to region where at least a gas structure went through. As soon as liquid, small bubbles and the biggest one pass alternatively at a given location, the entropy exceeds the 3-state threshold E_3. This particular value is indicated by black contours on entropy maps in figure 6 and the 3-state region is coloured in yellow to white. For the cavitation

inception regime (cond. 3 in figure 6), the contour E_3 delimits a zone that was covered by the biggest bubble at least one time in the image series. The maximum entropy remains around E_3 for this condition, meaning that the three states are not equally probable. Indeed, $(p_L, p_G, p_B) \approx (0.65, 0.25, 0.1)$ for this condition. For the other conditions, the 3-state contour delimits an inner region where $E < E_3$. In this region only two states are encountered, meaning that the cavitation plume is always present here. The entropy even reaches again zero for pixels only covered by the cavitation plume in the series. The regions $E > E_3$ surrounding the cavitation plume, and called the bubble detachment zone, are populated by small bubbles. The spreading of this zone is relatively large for regime III and greatly decreases for regime IV as can be seen also on the figure 7-a presenting the variation of the normalized bubble detachment zone area A_{BD} as a function of the flow rate. From cavitation inception to super cavitation regime a steep increase of A_{BD} occurs but it constantly decreases after with increasing flow rates. This results from stabilization of the cavitation plume. Indeed, in regime IV the main fluctuating part remains near the nozzle exit, on the downstream side. For this regime the cavitation plume represents around 70% of the nozzle area and the bubble detachment zone is only about 5-6% of it.
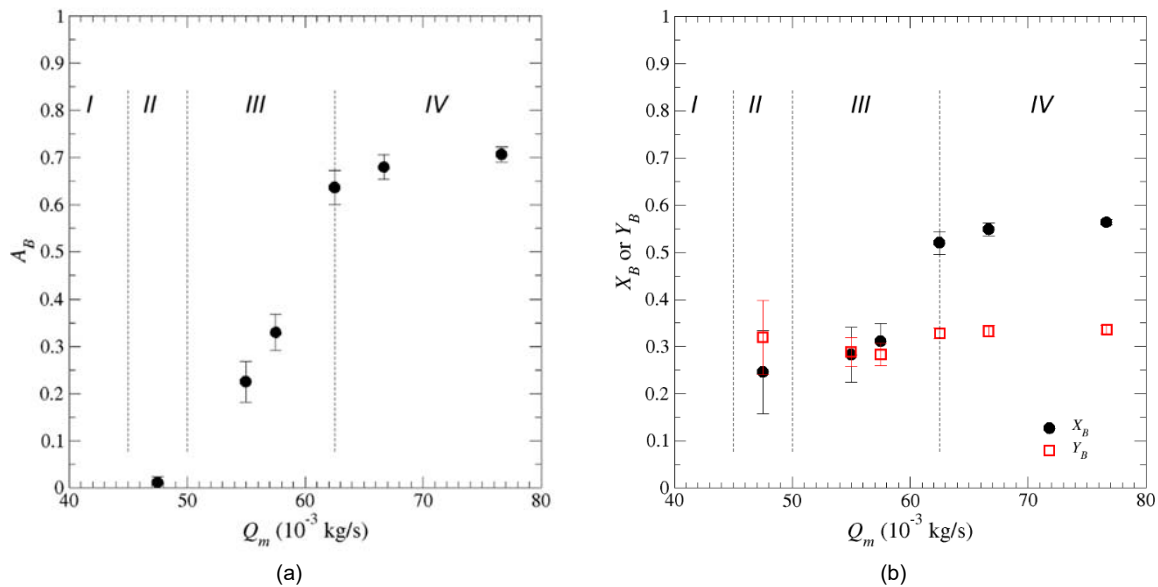
Figure 5. Internal flow: cavitation plume area A_B (a) and centroid coordinates (X_B, Y_B) (b) as a function of the flow rate. Error bars represent the standard deviation of the quantities over the image series.

Cond. 3 (II)   Cond. 4 (III)   Cond. 5 (III)   Cond. 6 (IV)   Cond. 7 (IV)   Cond. 8 (IV)
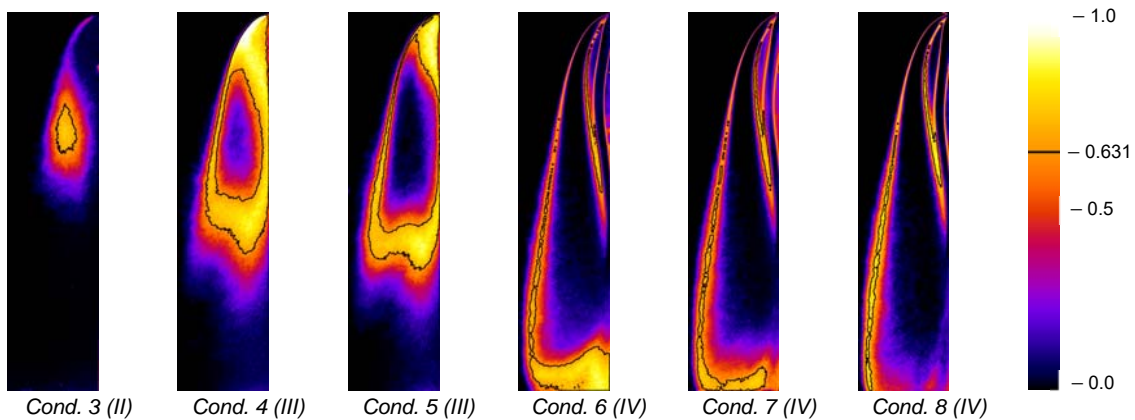
Figure 6. Internal flow: entropy maps for conditions 3 to 8 (regimes indicated in brackets). Correspondence between colours and entropy values are given in the right column. The black lines delimits the 3-state regions (E_3=0.631).

In regime IV it can be observed (see Fig. 6) that the limit between the liquid and the cavitation plume is very stable as the non-null entropy region is very thin, particularly near the nozzle entrance. The contours delimiting the non-null entropy regions are superimposed for all the conditions in the image of figure 7-b. On the left side of this image (red curve in figure 7-b) the boundary between the liquid and the bubbles is almost unaffected by the flow rate, and this, whatever the cavitation regime. Two contours (yellow and cyan) diverge a bit: they belong to regime III for which small bubbles in the detachment zone can be entrained in the liquid. This limit between liquid and vapour in the nozzle is clearly dominated by the streamlines of the liquid flow.

For the regime IV, two particular flows structures can be seen near the upstream side wall of the nozzle (see figures 6 and 7-c,d); 1 - a large vapour cavity and 2 - a re-entrant jet:

1 - Between the two vertical black strips attached to the upper upstream corner there is a grey region in the image (indicated by red arrows in figure 7-c,d). Even though this region is in light grey levels similar to the liquid region, it is not associated to liquid. Indeed, the local structure of the image clearly shows a wavy liquid-gas interface. This evidences the presence of a large gas cavity of width of the order of the width of the light grey level region and of thickness likely to be of the order of the nozzle thickness T_N. It is also suspected that the other parts of the cavitation plume associated to black regions in DBI images are rather composed of a two-phase structure with many gas-liquid interfaces as in foam.

2 – Another light grey region touching the upstream side wall is seen on the nozzle flow images. This second region is associated to liquid as the local grey level structure is identical to the light background. This evidence the presence of liquid in this region that is induced by a re-entrant jet [12][13]. The local movement of this re-entrant jet is oriented upstream, as seen from high speed visualizations. This re-entrant jet can be sometimes populated with vapour bubbles as can be seen on figure 7-d.

It is clear from the entropy maps that for the highest flow rates these two flow structures, large gas cavity and re-entrant jet, are stable in this region (null entropy). If there is no doubt about the liquid phase of the re-entrant jet, it is not clear if the large gas cavity is vapour or air. It is believed that this cavity is more likely to be full of vapour because it does not seem to extend down to the nozzle exit to allow air coming in the nozzle.

(a)   (b)   (c)   (d)
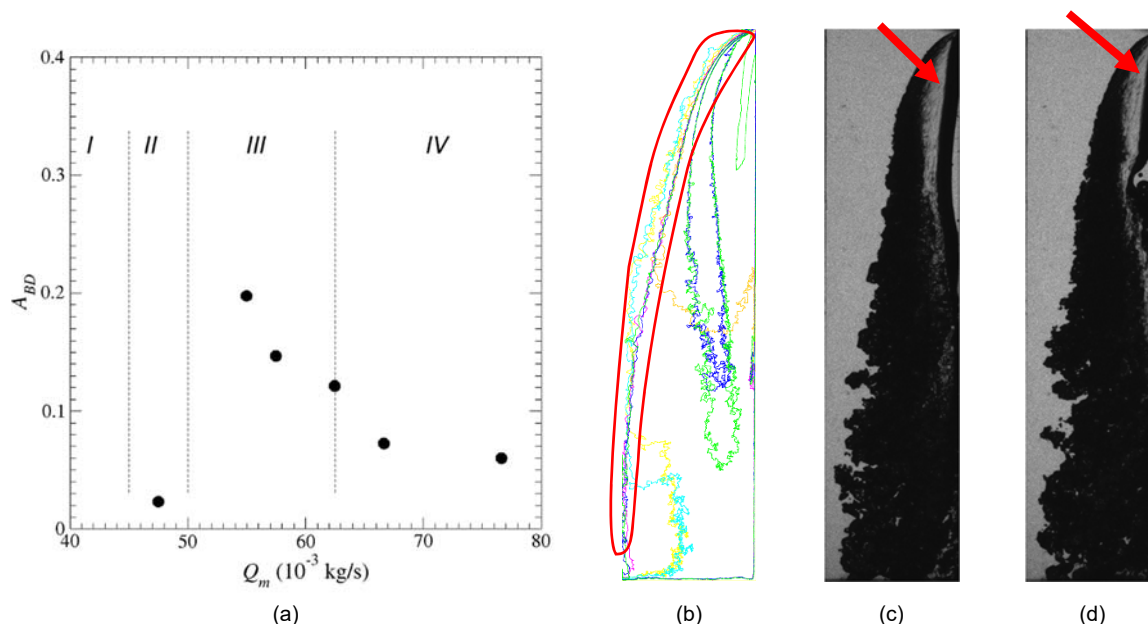
Figure 7. Internal flow: a - Normalized area of the bubble detachment region A_{BD} as a function of the flow rate; b – non-null entropy contours superimposed for the condition 3 to 8; c,d – images of the flow in condition 8.

External flow analysis

The external flow emanating from the nozzle is mainly a planar liquid sheet at the nozzle exit that disintegrates into ligament and droplets (see figure 3). The liquid jet is the biggest liquid element in the image that constitutes the state B. Entropy maps are presented in figure 8 for the external flow. The entropy is null for the flow regions always occupied by the air or by the jet. The coloured regions in entropy maps (i.e. non-null entropy values) correspond to region where at least one dispersed droplet was seen. As soon as air, droplets and the liquid jet alternatively occupy a given location, the local entropy value exceeds the 3-state threshold E_3 and the associate region is called the primary atomisation zone. Black contours delimit this zone on entropy maps in figure 8. It is clearly seen that for regimes I to III, the 3-state region is far less extended on the downstream side (left side) as transition from air to jet occurs with almost no droplets between, i.e. the primary atomisation zone is reduced to its minimum.

On the upstream side the atomization expands a bit more, particularly for regime III and IV. In fact, the primary atomization zone area A_a starts decreasing when cavitation inception regime is reached and then increases as flow rate increases for both jet sides, as can be seen in figure 9-a. Moreover, whereas this area increases between regimes II to IV, it decreases again at maximum flow rate. It can be observed also that the downstream side area is far smaller than the upstream one.

The reason for the first decrease of the primary atomization area (from regime I to II) can be assigned to a modification on the internal liquid flow that could lead to a less efficient atomization or to an atomization area shifted farther downstream from the orifice outlet. The second decrease observed in regime IV occurs when the cavitation plume permanently reaches the outlet. A complete reorganization of the atomization process happens under this

condition, leading to an apparently decreasing atomization area in the images but with an increase of the atomization in the perpendicular direction as can be seen on perpendicular views shown in figure 10. No entropy analysis was however possible for these perpendicular views for which only 50 images were recorded.

Cond. 2 (I) *Cond. 3 (II)* *Cond. 5 (III)* *Cond. 7(IV)*
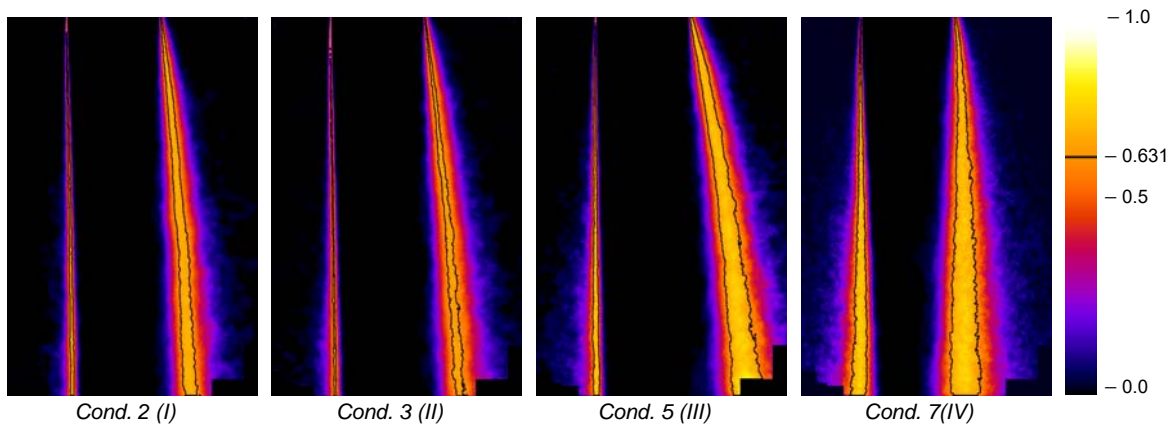
Figure 8. External flow: entropy maps for conditions 2, 3, 5 and 7. Correspondence between colours and entropy values are given in the right column. The black lines delimits the 3-state regions (E_3=0.631).

The primary atomization area is characterized by the presence of dispersed droplets which is quantified by measuring the area A_d of the region where the probability of presence of droplets is greater than 2.5%. The results are reported in figure 9-b. It can be noticed that this region expand beyond the primary atomization area (i.e. $A_d \approx 3 \times A_a$) as droplet can be encountered in regions where the jet never comes. The same trends are observed for this droplet region than for the primary atomization area, i.e. its area is far smaller for the downstream side and it increases with the flowrate except at large flow rates where A_d goes back to value corresponding to the regime III.

(a) (b)
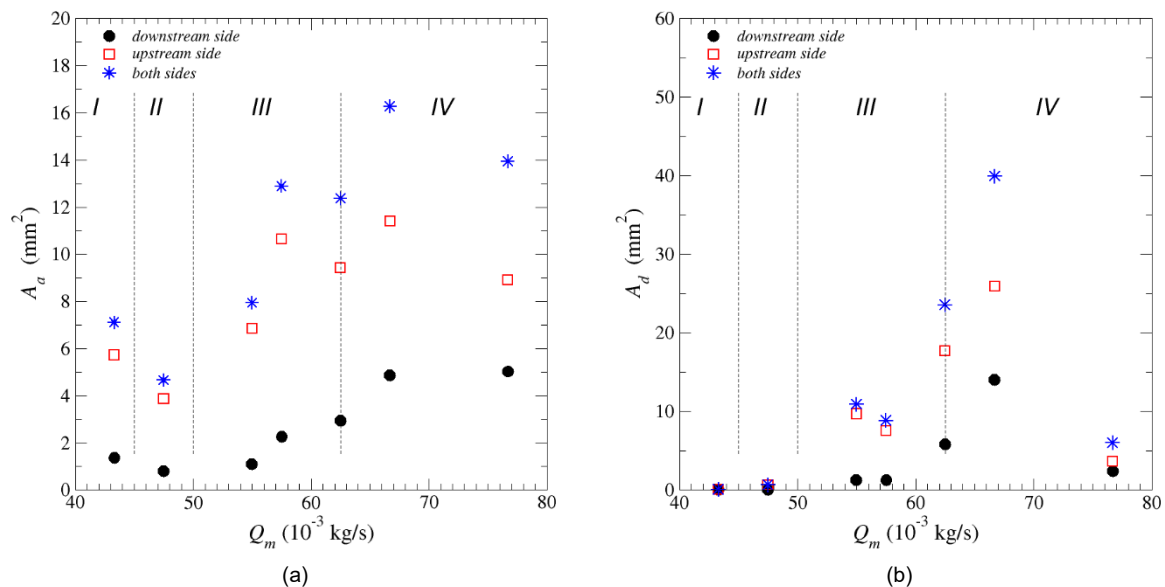
Figure 9. External flow: a – primary atomization zone and b – droplet probability areas as functions of flow rate.

Internal-external correlations

By comparing the quantitative results for internal and external flows it is possible to deduce some correlations. The size of the cavitation plume seems to correlate to the primary atomization area. This is not surprizing as it is well admitted that cavitation could have a non-negligible effect on the atomization process. We correlate here the cavitation activity to the cavitation plume area and the atomization efficiency to the primary atomization area.

The decrease noticed for the primary atomization zone area and for the droplet area at the highest flow rate is linked to a reorganization of the atomization process. This correlate to the reduction of the bubble detachment zone area and to the stabilization of the bubble plume in the nozzle orifice. It is however not possible to correlate this to properties of the internal flow in this perpendicular direction as no visualization can be made in this direction due to the plain plates from which the nozzle is made.
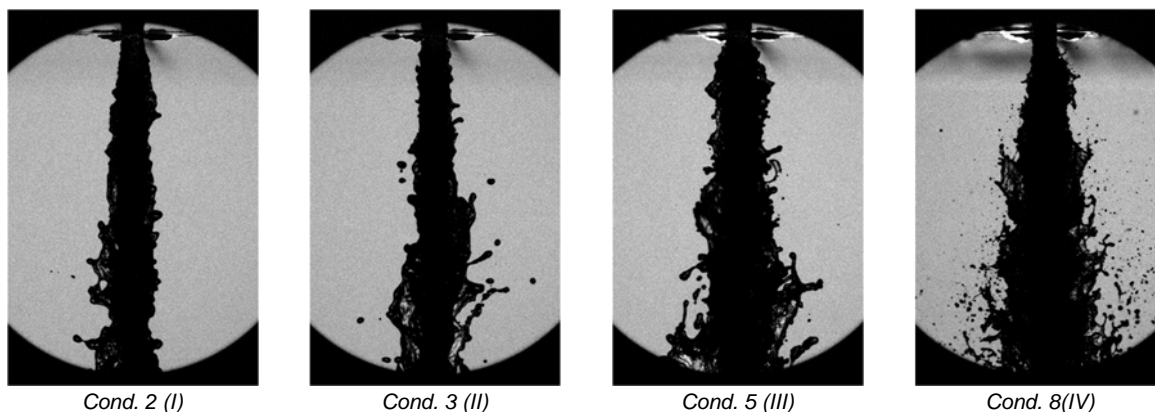
| *Cond. 2 (I)* | *Cond. 3 (II)* | *Cond. 5 (III)* | *Cond. 8(IV)* |

Figure 10. External flow: Perpendicular view of the jet.

Conclusions

The entropy approach presented in this article is shown to be an efficient way to quantitatively characterize processes such as cavitation and atomization. Some very stable behaviours are thus evidenced from the analysis of entropy maps, including the stable location of the interface between liquid and vapour phase, of the re-entrant jet or of the large gas cavity observed in the cavitation plume at high flow rates. Statistics relative to the observed phenomenon, here cavitation and atomization, are quantitatively characterized through the measurement of region area. By defining the bubble detachment region or the primary atomization region from the local entropy value, it was possible to quantify the cavitation activity and the atomization efficiency. The cavitation plume is found to increase with increasing the flow rate whereas the bubble detachment region area decreases for the highest flow rates. This is accompanied with a reorganization of the atomization in the jet.

Acknowledgements

References

[1]   Dabiri, S., Sirignano, W. A., Joseph, D. D., 2007, Phys. Fluids, 19, 072112.

[2]   Payri, F., Bermudez, V., Payri, R., Salvador, F. J., 2004, Fuel, 83, 419-431.

[3]   Desantes, J. M., Payri, R., Salvador, F. J., De la Morena, J., 2010, Fuel, 89, 3033-3041.

[4]   Cao, Y., Idlahcen, S.,Blaisot, J. B., Rozé, C., Méès, L., Maligne, D., Sep. 6.-8. 2017, 28th European Conference on Liquid Atomization and Spray Systems.

[5]   Arcoumanis, C., Flora, H., Gavaises, M., Badami, M., 2000, SAE 2000-01-1249.

[6]   Mitroglou, N., Stamboliyski, V., Karathanassis, I., Nikas, K., Gavaises, M., 2017, Experimental Thermal and Fluid Science, 84, 179-189.

[7]   Sou, A., Maulana, M. I., Isozaki, K., Hosokawa, S., Tomiyama, A., 2008, Journal of Fluid Science and Technology, 3, 622-632.

[8]   Payri, R., García, J., Salvador, F., Gimeno, J., 2005, Fuel, 84, 551-561.

[9]   Mauger, C., Méès, L., Michard, M., Azouzi, A., Valette, S., 2012, Exp. Fluids, 53, 1895-1913.

[10]   Sou, A., Pratama, R. H., Tomisaka, T., Kibayashi, Y., Sep. 2.-6. 2012, 12th triennial international conference on liquid atomization and spray systems.

[11]   Blaisot, J. and Yon, J., Sep. 6.-8. 2004, 19th ILASS-Europe, 118-123.

[12]   Dular, M., Khlifa, I., Fuzier, S., Adama Maiga, M., Coutier-Delgosha, O., 2012, Exp. Fluids, 53, 1233-1250.

[13]   Stanley, C., Barber, T., Milton, B., Rosengarten, G., 2014, Int. J. Heat Fluid Flow, 50, 169-176.